On the Equilibrium of a Linear Extrap Pinch

B. Lehnert
Royal Institute of Technology, Stockholm, Sweden

Z. Naturforsch. **37a**, 769–779 (1982); received September 26, 1981

To Professor Arnulf Schlüter on his 60th Birthday

The equilibrium is studied of a pinched linear plasma column of "Extrap" type which is confined in a purely transverse magnetic field, partly arising from currents in a set of external conductor rods being introduced for stabilizing purposes. The axial and transverse losses are separated in a simplified theoretical model for which stability is assumed as a working hypothesis and anomalous transport as well as impurity radiation are neglected. Then, the reduction of the axial heat transport by the magnetic field will have a substantial effect on the over-all heat balance, thus leading to high temperatures at large axial lengths of the plasma column. Conditions near ignition should become possible at technically realistic linear dimensions and pinch currents.

1. Introduction

In research on controlled fusion, substantial progress has been made within the field of magnetic confinement during the last decade. Nevertheless there remain fundamental plasma physical and fusion technological problems to be solved before a technically feasible and economically competitive fusion reactor can be realized. Further progress therefore requires considerable efforts to be made also on lines being alternative to that of the tokamak concept, such as on advanced stellarators [1], compact toroids, reversed-field pinches, multipoles, Z-pinches, and on new trends in open confinement.

Among these alternative lines, a high-beta scheme, "Extrap", has recently been investigated [2, 3] which consists of a toroidal Z-pinch immersed in the transverse (poloidal) magnetic field being produced by currents in a set of external ring-shaped conductors. Research on Extrap is still at an early stage, as represented by an incomplete theory and experiments on small scale. This paper is restricted to part of the equilibrium problems of a linear Extrap system of finite length, with special emphasis on the possibility of reaching ignition. One example of such a system with four external conductors is outlined in Figure 1.

In an ideal magnetic bottle, the guiding centre orbits form closed paths both in the directions along and across the magnetic field. Such conditions can be realized by closed toroidal schemes with a main poloidal field, as well as in advanced stellarators [1]. The complexity of toroidal geometry can in two ways be diminished at the expense of a reduced confinement. The first is represented by open bottles, such as mirror devices, where the transverse guiding-centre motion still forms closed orbits, but part of the plasma particles are lost along the field lines. The second way is represented by straight geometries in which the magnetic field lines are closed within the confinement volume, but where the guiding-centre motions across the field lines lead out to surrounding vessel walls. This second type of scheme

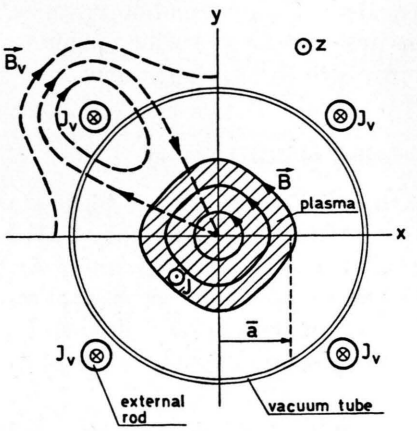

Fig. 1. Outline of the cross-section of a linear Extrap configuration with four conductor rods. A purely transverse confinement field $\boldsymbol{B} = \boldsymbol{B}_p + \boldsymbol{B}_v$ is created by the plasma current density $\boldsymbol{j} = \text{curl}\, \boldsymbol{B}_p/\mu_0$ and the currents J_v in the rods. The pattern of the field $\boldsymbol{B}_v$ generated by the rod currents is shown in the upper left-hand part of the figure.

Reprint requests to Prof. Bo Lehnert, Department of Plasma Physics and Fusion Research, Royal Institute of Technology, 10044 Stockholm, Schweden.

0340-4811 / 82 / 0800-0769 $ 01.30/0. — Please order a reprint rather than making your own copy.

includes ordinary and hardcore pinches without an axial magnetic field, as well as linear "Extrap" devices.

The confinement of a straight plasma column by a purely transverse magnetic field does not only represent a first step towards closed toroidal geometry, but also has some merits of its own. Thus, in a strong magnetic field the end losses due to the transverse guiding-centre motions become much smaller than the end losses in simple mirror machines, at least in certain parameter ranges such as those of high plasma densities. Since the field lines do not intersect the end electrodes in a pinch configuration of the present type, the particle and heat transport to the electrodes also becomes much smaller than in straight pinches which are stabilized by an axial magnetic field. In other words, the reduced axial transport in straight Extrap geometry and similar schemes allows for axial temperature gradients and high temperatures within parts of the plasma column. Also the axial impurity transport from the electrode surfaces becomes reduced, as compared to that arising in systems with an axial magnetic field component. Further, steady confinement becomes possible at high beta values, by feeding strong d.c. currents between the end electrodes.

The linear Z pinch has been subject to an earlier analysis by Haines [4] in terms of MHD theory of a plasma with equal ion and electron temperatures. This paper forms an extension of such an analysis, with special emphasis to the Extrap scheme.

2. On the Applicability of MHD Theory

The linear Extrap pinch of Fig. 1 is a high-beta system with vanishing magnetic field strength $\boldsymbol{B}$ at the axis $x = y = 0$. When the mean free path is large compared to the macroscopic dimensions, application of MHD theory in terms of localized small volume elements becomes questionable at least in three respects:

(i) The Larmor radii of ions and electrons tend to infinity at the axis.

(ii) At high temperatures and at beta values of order unity, the ion Larmor radius can become comparable to the characteristic macroscopic dimensions also within the main and outer parts of the plasma volume.

(iii) The non-circular plasma cross section leads to spatial variations along the magnetic field lines, the integrated (non-localized) effect of which has to be taken into account in a rigorous theory.

To discuss these questions of applicability more in detail, some general features of the system first have to be outlined. Let ψ denote the flux function of the magnetic surfaces of the field $\boldsymbol{B}$ in Figure 1. Using SI-units,

$$\mu_0 J(\psi) = 2\pi \bar{r}(\psi)\, \bar{B}(\psi), \tag{1}$$

where $J(\psi)$ is the total current enclosed by a surface $\psi = \text{const}$, $B = |\boldsymbol{B}|$, $r(\psi)$ is the axial distance of a point at the same surface, and

$$\bar{Q} = \oint Q\, \mathrm{d}s / \oint \mathrm{d}s$$

for any quantity Q being integrated along a closed field line with line elements $\mathrm{d}s$. In the case of large heat conduction along $\boldsymbol{B}$, the plasma temperature $T = T(\psi)$ and the average ion Larmor radius become related by

$$\bar{a}_\mathrm{i}(\psi) = [2 m_\mathrm{i} k T(\psi)]^{1/2} / e \bar{B}(\psi). \tag{2}$$

The effective characteristic macroscopic length $\bar{L}_\mathrm{c}$ is further defined by

$$1/\bar{L}_\mathrm{c} \equiv 1/\bar{r}(\psi) + 1/\bar{L}_\mathrm{p}(\psi), \tag{3}$$

where $\bar{L}_\mathrm{p}(\psi)$ represents the characteristic length of the plasma variations in the direction across the magnetic surfaces. Combination of (1)—(3) yields a relative magnitude of the ion Larmor radius

$$\varrho_\mathrm{i} \equiv \bar{a}_\mathrm{i}/\bar{L}_\mathrm{c} = C_\mathrm{i} T_0^{1/2} F(\psi)/J(\psi);$$
$$F = [1 + (\bar{r}/\bar{L}_\mathrm{p})]\, f^{1/2}, \tag{4}$$

where $C_\mathrm{i} = (8\pi^2 m_\mathrm{i} k)^{1/2}/\mu_0 e \cong 6.70\sqrt{A}$, with A indicating the mass number and $T_0 = T/f$ standing for the plasma temperature at the axis. For plasma parameter distributions of physical interest we have $f \cong 1$, $\bar{r} \ll \bar{L}_\mathrm{p}$ and $F \cong 1$ close to the axis, whereas f and $\bar{L}_\mathrm{p}$ usually decrease with increasing $\bar{r}$.

In the case of parabolic and similar distributions, the factor F deviates only moderately from unity within the main parts of the plasma volume. Under such circumstances a crude estimate of the range of validity of MHD theory is obtained by putting $F \cong 1$ and $\varrho_\mathrm{i} \leqq \varepsilon \ll 1$ which yields the condition

$$J \geqq J_\mathrm{c} \cong C_\mathrm{i} \sqrt{T_0}/\varepsilon. \tag{5}$$

As an example we put $\varepsilon = 0.2$, say, and obtain a critical current $J_\mathrm{c} \cong 0.5$ MA for a deuterium-tritium mixture at thermonuclear temperatures

$T \cong 10^8$ K. In this case MHD theory can at best be applied only to the outer layers of a pinched plasma column which carries a considerable total current.

Consequently, the previous points (i) and (ii) could be disregarded only when condition (5) is satisfied, and point (iii) when there are small deviations from a circular plasma cross section. With these limitations in mind, MHD theory will be used in the following sections to give a first indication on the behaviour of the plasma in the present equilibrium state. The later obtained results from MHD theory will also be partly supported by particle orbit theory which is independent of such limitations.

3. Starting Points of Analysis

A steady state is assumed to be reached and plasma stability is accepted as a working hypothesis which is also supported by recent experiments on Extrap devices at sufficiently strong currents in the external conductor rods [2, 3].

3.1. General Assumptions

The steady equilibrium of a quasi-neutral pure plasma of particle density n is treated on the basis of the following general assumptions:

(i) The axial length L of the plasma column is much larger then the average radius $\bar{a}$ of its cross section.

(ii) The inertia forces due to a macroscopic flow of the plasma are neglected. This is usually a good approximation when the fluid velocity remains much smaller than the thermal velocity of ions.

(iii) The density n is large enough for the plasma to become "impermeable" to neutral gas. Thus, narrow partially ionized boundary regions are created, both in the form of a cold-mantle surrounding the cylindrical surface of the plasma column in the xy plane of Fig. 1, and in the form of thin layers at the electrode surfaces bounding the plasma column in the axial z direction. Only the balance of the fully ionized part of the plasma body will be treated more in detail, whereas a short discussion on plasma-neutral gas interaction is postponed to Sects. 3.4 and 5.4.

(iv) The pinch current J is assumed to be strong enough for MHD analysis to become applicable to the main parts of the plasma volume, as specified in Section 2. Thus, only the weak-field region close to the pinch axis is excluded from the present macroscopic analysis. Still a rough picture of the plasma behaviour in this region becomes available from orbit theory. Further, the weak-field region could, in principle, give rise to enhanced axial losses of particles having velocities nearly directed along the axis, but these particles are not expected to be of crucial importance at large axial lengths L. In any case, the axial losses of these particles are included in the axial pinch current, as demonstrated later in Sects. 4.2 and 5.1. Finally, the large ion Larmor radius in the weak-field region introduces a kind of scattering and diffusion effect which tends to "smear out" the gradients and fluctuations of the plasma density and temperature near the axis [2].

(v) The present analysis is restricted to the optimum case where there is no substantial enhancement of the transport by anomalous effects. Especially in high-beta systems, this question has to be further analysed [5].

(vi) In its numerical applications this paper is limited to pinch radii of the order of $\bar{a} \cong 10^{-2}$ m, currents $3 \times 10^4 < J < 3 \times 10^6$ A, axial temperatures $3 \times 10^5 < (T_{i0}, T_{e0}) < 10^8$ K and axial densities $3 \times 10^{21} < n_0 < 10^{24}$ m^{-3}.

3.2. Basic Equations

Due to the antiparallel axial drift motions of ions and electrons in a system of finite axial length, it is often necessary to distinguish between the ion and electron temperatures T_i and T_e. We therefore adopt macroscopic two-fluid equations of the simplified form [6—9]

$$\operatorname{div}(n \boldsymbol{v}_i) = \operatorname{div}(n \boldsymbol{v}_e) = 0\,, \tag{6}$$

$$\begin{aligned} 0 = {} & e n (\boldsymbol{E} + \boldsymbol{v}_i \times \boldsymbol{B}) \\ & - \boldsymbol{\nabla} p_i - e^2 n^2 \eta (\boldsymbol{v}_i - \boldsymbol{v}_e) \\ & - (3 n^2 k e \eta / 2 B^2)(\boldsymbol{\nabla} T_e) \times \boldsymbol{B}\,, \end{aligned} \tag{7}$$

$$\begin{aligned} 0 = {} & - e n (\boldsymbol{E} + \boldsymbol{v}_e \times \boldsymbol{B}) \\ & - \boldsymbol{\nabla} p_e + e^2 n^2 \eta (\boldsymbol{v}_i - \boldsymbol{v}_e) \\ & + (3 n^2 k e \eta / 2 B^2)(\boldsymbol{\nabla} T_e) \times \boldsymbol{B}\,, \end{aligned} \tag{8}$$

$$\begin{aligned} & \tfrac{3}{2} \operatorname{div}(p_i \boldsymbol{v}_i) + p_i \operatorname{div} \boldsymbol{v}_i \\ & = 3 e^2 n^2 \eta (k/m_i)(T_e - T_i) - \operatorname{div} \boldsymbol{q}_i + \Pi_t\,, \end{aligned} \tag{9}$$

$$\tfrac{3}{2}\operatorname{div}(p_e \boldsymbol{v}_e) + p_e \operatorname{div} \boldsymbol{v}_e = -3e^2 n^2 \eta (k/m_i)(T_e - T_i) - \operatorname{div} \boldsymbol{q}_e + \eta j^2 - \Pi_r . \quad (10)$$

Here $\boldsymbol{v}_i$, $\boldsymbol{v}_e$ are the fluid velocities of ions and electrons, $\boldsymbol{E}$ and $\boldsymbol{B}$ the electric and magnetic fields, $p_i = n k T_i$, $p_e = n k T_e$, $\boldsymbol{q}_i$, $\boldsymbol{q}_e$ the heat flow vectors, and $\boldsymbol{j}$ the current density. Further, with ν_{ei} and ν_{ii} as the electron-ion and ion-ion collision frequencies, the resistivity $\eta = m_e \nu_{ei}/e^2 n$ has the value $\eta_\perp = k_\eta / T_e^{3/2}$ across $\boldsymbol{B}$ with $k_\eta = 129$ ($\ln \Lambda$), and the ion heat conductivity becomes $\boldsymbol{q}_i = \boldsymbol{q}_{i\perp} \cong -\lambda^* \nabla_\perp T_i$ across $\boldsymbol{B}$ with

$$\lambda^* = 5 n k^2 T_i m_i \nu_{ii}/4 e^2 B^2 = k_2 n^2 \sqrt{A}(\ln \Lambda)/B^2 \sqrt{T_i}$$

and $k_2 \cong 1.5 \times 10^{-42}$. Finally

$$\Pi_t = f_\alpha k_t n^2 \varrho_t \quad (11)$$

is the thermonuclear reaction power being shared by charged constituents where

$$f_\alpha \cong 0.2 , \quad k_t \cong 7.05 \times 10^{-13}$$

joules for the DT-reaction, ϱ_t is the corresponding reaction rate [10], and

$$\Pi_r = k_{rb} n^2 \sqrt{T_e} + k_{rc} n B^2 T_e \quad (12)$$

is the loss due to bremsstrahlung and unabsorbed cyclotron radiation [11] with

$$k_{rb} \cong 1.7 \times 10^{-40} , \quad k_{rc} \cong 8 \times 10^{-24} , \quad Z = 1$$

throughout this paper, and the rest of the symbols having their conventional meaning.

With $m = m_i + m_e$, the substitutions

$$\boldsymbol{v}_i = \boldsymbol{v} + (m_e/e n m)\boldsymbol{j} , \quad \boldsymbol{v}_e = \boldsymbol{v} - (m_i/e n m)\boldsymbol{j}$$

and $p = p_i + p_e$, eqs. (6)—(10) combine to

$$\operatorname{div}(\boldsymbol{n} v) = 0 , \quad \operatorname{div} \boldsymbol{j} = 0$$

and

$$\boldsymbol{j} \times \boldsymbol{B} = \nabla p , \quad (13)$$

$$\eta \boldsymbol{j} = \boldsymbol{E} + \boldsymbol{v} \times \boldsymbol{B} - (1/e n m)(m_i \nabla p_i - m_e \nabla p_e) + (3 n k \eta / 2 B^2) \boldsymbol{B} \times \nabla T_e , \quad (14)$$

$$\tfrac{3}{2} \operatorname{div}(p \boldsymbol{v}) + p \operatorname{div} \boldsymbol{v} - (3/2 e m) \operatorname{div}[(m_i p_e - m_e p_i)\boldsymbol{j}/n] - (m_i p_e - m_e p_i) \operatorname{div}(\boldsymbol{j}/e n m) = \eta j^2 - \operatorname{div}(\boldsymbol{q}_i + \boldsymbol{q}_e) + \Pi_t - \Pi_r . \quad (15)$$

3.3. *The Relative Magnitude of the Heat Conduction Loss*

When anomalous transport can be neglected, heat conduction is mainly due to the ions. For large pinch lengths $L \gg \bar{a}$ the corresponding heat loss is mainly directed in the transverse direction of the plasma column. With subscripts (0) and (b) denoting the axis and the boundary region of the column, respectively, an order-of-magnitude estimation yields a ratio between the total heat conduction loss and the total ohmic heating power

$$\Lambda \equiv \Pi_\lambda / \Pi_\eta \cong k_\Lambda (\bar{a}/L_{Tb}) \cdot (T_b/T_0)^{1/2} (n_b/n_0)^2 . \quad (16)$$

Here

$$\Pi_\lambda = \int \operatorname{div} \boldsymbol{q}_i \, dV \quad \text{and} \quad \Pi_\eta = \int \eta j^2 \, dV$$

are integrals over the plasma volume V,

$$k_\Lambda \cong 10 \sqrt{A} , \quad L_{Tb} \equiv T/|\nabla T|$$

in the boundary region, the approximation $T_i \cong T_e \equiv T$ has been adopted, and use has been made of eq. (13) in the present high-beta case. In connection with eq. (16) the following points should be made:

(i) The condition $\Lambda < 1$ for ohmic heating to cover the heat conduction loss should become satisfied for plasma columns having a sufficiently large radius and magnetic field strength. This allows for a large pressure difference between the core and the boundary, such as to make $T_b \ll T_0$ and $n_b \ll n_0$ at values $\bar{a}/L_{Tb}$ of order unity.

(ii) In a general situation the condition $\Lambda < 1$ neither becomes necessary nor sufficient for a steady heat balance to exist. Thus, there are heat sources in addition to ohmic heating, also including those from the frictional work of macroscopic fluid motions [5], and there are heat sinks in addition to that from heat conduction, also including convective losses from fluid motions [5].

3.4. *Influence of Neutral Gas Interaction on the Heat Balance*

The penetration length of fast neutral particles [12] becomes $L_{nf} = 1/n\sigma_{cf}$ where $1/\sigma_{cf} \cong 5 \times 10^{18}\,\mathrm{m}^2$ at plasma temperatures exceeding $T_b \cong 5 \times 10^4\,\mathrm{K}$. The corresponding impermeability condition $n_0 \bar{a} \gg 1/\sigma_{cf}$ is thus seen to be satisfied within the parameter ranges given by Section 3.1.(vi). In par-

ticular with n_{nb} as the value of the neutral gas density n_n at the boundary of the plasma and with the coordinate ζ being perpendicular to the boundary and pointing into the plasma body, the local distribution of neutrals becomes

$$n_n = n_{nb} \exp(-n \sigma_{ct} \zeta).$$

The influence of the neutral gas on the heat balance can then be included by subtracting a term

$$\begin{aligned} \Pi_n &= n n_n [e \varphi_i \xi + \tfrac{3}{2} k (\varrho_{in} T_i + \varrho_{en} T_e)] \\ &\equiv n n_n Q_n \end{aligned} \tag{17}$$

from the right-hand member of (15). Here φ_i stands for the ionization potential, ξ for the ionization rate, and ϱ_{in}, ϱ_{en} for the reaction rates of ions and electrons due to all other impacts with the neutrals than those leading to ionization. The influence of Π_n can be estimated by comparing it with the ohmic heating power. For $\zeta = \bar{a}$, it is easily seen that $\Pi_n / \eta j^2 \ll 1$ in the parameter ranges given in Section 3.1.(vi). Then, the heat balance in the hot plasma core should hardly be affected by neutral gas interaction. On the other hand, such interaction should have an influence in the end electrode layers, to which we return later in this paper.

4. Particle and Momentum Balance

4.1. The Field Geometry

In the special case of a plasma column of circular symmetry in a cylindrical frame $(r \varphi z)$, the current density and the transverse magnetic field would have the general forms $\boldsymbol{j} = (j_r, 0, j_z)$ and $\boldsymbol{B} = (0, B, 0)$ when the plasma cross section is assumed to vary in thickness in the axial z direction. From the curl of (13) it is seen, however, that $\partial B / \partial z = 0$ and $j_r = 0$, i.e. $\boldsymbol{j} = [0, 0, j(r)]$ and the plasma column therefore has to be uniform in the axial direction.

In the more general case of a non-circular plasma cross section, the balance equations are also satisfied by $j_x = 0$, $j_y = 0$, $B_z = 0$ in the frame (xyz) of Figure 1. Throughout this paper we thus restrict ourselves to columns of uniform cross section in the axial direction. As a consequence, $\partial j / \partial z = 0$ and (13) yields $\boldsymbol{j} \cdot \nabla p = 0$ from which

$$\partial / \partial z [n (T_i + T_e)] = 0. \tag{18}$$

The present field geometry leads to $\boldsymbol{j} \cdot \boldsymbol{B} = 0$. (13) further gives $\boldsymbol{B} \cdot \nabla p = 0$. Within the parameter ranges of interest in this connection, the assumption of a constant electric potential along $\boldsymbol{B}$ should become a valid approximation. Equations (7) and (8) then yield $\boldsymbol{B} \cdot \nabla p_i = 0$ and $\boldsymbol{B} \cdot \nabla p_e = 0$. If, in addition, the thermal conductivity due to the electron motion along $\boldsymbol{B}$ is high enough for $\boldsymbol{B} \cdot \nabla T_e \cong 0$, we also have

$$\boldsymbol{B} \cdot \nabla n \cong 0 \quad \text{and} \quad \boldsymbol{B} \cdot \nabla T_i \cong 0.$$

It is finally observed that there are no accelerating forces of the ion and electron fluid motions along $\boldsymbol{B}$. Consequently, $\boldsymbol{B} \cdot \boldsymbol{v}_i = 0$ and $\boldsymbol{B} \cdot \boldsymbol{v}_e = 0$. When using the symbols $\boldsymbol{v}_i$, $\boldsymbol{v}_e$, $\boldsymbol{v}$, $\boldsymbol{j}$, and ∇ in the coming sections, it should therefore be kept in mind that they refer to the directions being perpendicular to $\boldsymbol{B}$ only.

4.2. Fluid and Guiding Centre Motions

Equations (7), (8), (13) and (14) combine to

$$\begin{aligned} \boldsymbol{v}_i &= \boldsymbol{v} + (m_e \boldsymbol{B} / e n m B^2) \times \nabla p \\ &= \boldsymbol{E} \times \boldsymbol{B} / B^2 + (\boldsymbol{B} / e n B^2) \times \nabla p_i \\ &\quad - (\eta / B^2)(\nabla p - \tfrac{3}{2} n k \nabla T_e), \end{aligned} \tag{19}$$

$$\begin{aligned} \boldsymbol{v}_e &= \boldsymbol{v} - (m_i \boldsymbol{B} / e n m B^2) \times \nabla p \\ &= \boldsymbol{E} \times \boldsymbol{B} / B^2 - (\boldsymbol{B} / e n B^2) \times \nabla p_e \\ &\quad - (\eta / B^2)(\nabla p - \tfrac{3}{2} n k \nabla T_e), \end{aligned} \tag{20}$$

$$\begin{aligned} \boldsymbol{v} &= \boldsymbol{E} \times \boldsymbol{B} / B^2 + (\boldsymbol{B} / e n m B^2) \\ &\quad \times (m_i \nabla p_i - m_e \nabla p_e) \\ &\quad - (\eta / B^2)(\nabla p - \tfrac{3}{2} n k \nabla T_e). \end{aligned} \tag{21}$$

We now turn to the case $T_i \cong T_e \equiv T$, the conditions of which will be investigated in Section 5. Introducing subscripts $(_z)$ and $(_t)$ for the axial and transverse ("radial") directions of the plasma column, and observing that

$$|\nabla_t n| \gg |\nabla_z n|, \quad |\nabla_t T| \gg |\nabla_z T|$$

when $L \gg \bar{a}$, (21) can be rewritten as

$$\boldsymbol{v}_z \cong \boldsymbol{E}_t \times \boldsymbol{B} / B^2 + (1/2 e n B^2) \boldsymbol{B} \times \nabla_t p, \tag{22}$$

$$\begin{aligned} \boldsymbol{v}_t &= \boldsymbol{E}_z \times \boldsymbol{B} / B^2 \\ &\quad - (\eta k / 2 B^2 n^3) \nabla_t (n^4 T), \end{aligned} \tag{23}$$

where $\boldsymbol{v} = \boldsymbol{v}_z + \boldsymbol{v}_t$. Concerning the components $\boldsymbol{v}_z$ and $\boldsymbol{v}_t$ of the centre-of-mass velocity $\boldsymbol{v}$, the following points should be made:

(i) In the axial direction the basic equations (6) to (15) allow, in principle, for an un-accelerated axial mass motion $\boldsymbol{v} = (0, 0, v_z)$. However, there are reasons to assume this motion to be negligible,

because the ions entering the plasma column are formed from neutral particles of low temperature in the anode region and are starting there in cycloid-like orbits at their time of creation. Provided that there is no excessively large electric field within this region, it is then justified to assume corresponding initial value of v_z to be small. In addition, $\operatorname{div}(n\boldsymbol{v}) = 0$ yields $\partial(n v_z)/\partial z = 0$ and $\partial n/\partial z = 0$ for $v_z = \text{const} \neq 0$. In combination with (18) this would lead to the singular case $\partial(T_i + T_e)/\partial z = 0$ which has no physical interest in this connection. Therefore we have to put $v_z \equiv 0$. Due to (22) this implies that the pressure gradient $\nabla_t p$ is balanced by an ambipolar electric field $\boldsymbol{E}_t \cong -(1/2\,e\,n)\nabla_t p$. Provided that these conclusions hold also in the presence of impurities which are released from the electrodes, the condition $v_z = 0$ further implies that axial transport of these impurities into the hotter parts of the plasma column becomes strongly delayed.

(ii) In the transverse direction eq. (23) shows that there are two contributions to the fluid motion. The first is an inward directed drift due to the axial electric field $\boldsymbol{E}_z$ which drives the pinch current density $\boldsymbol{j}$ as indicated in Figure 1. The second is a transverse diffusion velocity due to the combined action of the pressure gradient ∇p and the Nernst term $(3\,n\,k/2)\nabla T$ appearing in the last bracket of (21). In cases where $\nabla_t(n^4 T)$ is directed towards the column axis, it thus counteracts the inward drift motion due to $\boldsymbol{E}_z$. With subscript $(_t)$ defining the outward normal direction of the magnetic surfaces $\psi = \text{const}$, (23) can be rewritten as

$$B v_t = E_{pN} - E_z; \quad E_{pN} \equiv \eta\, n\, k\, T/2\, B L_t, \tag{24}$$

where $L_t \equiv -n^4 T/\nabla_t(n^4 T)$. Restricting ourselves to positive values of $L_t \propto \bar{a}$ and to a constant number of particles per unit length of the plasma column, we have $E_{pN} \propto 1/BT^{1/2}\bar{a}^3$. For variations in the average pinch radius $\bar{a}$, and when $BT^{1/2}$ changes more slowly with $\bar{a}$ than $\bar{a}^3$, it is then seen that E_{pN} increases at a decreasing radius $\bar{a}$ and vice versa. For a constant applied electric field E_z (24) is thus expected to have a "stable" equilibrium at $v_t = 0$, with respect to variations of $\bar{a}$. The outward diffusion by the pressure and Nernst effects is then cancelled by the inward drift due to the axial electric field. The equilibrium $v_t = 0$ is independent of the inclusion of viscous forces in the pressure tensor. Finally, from (13) and (14) is seen that this equilibrium becomes consistent with the conventional Bennett relation between the pinch current J and the radius $\bar{a}$. The following deductions of this paper are therefore limited to the case $v_t \equiv 0$. The more general situation leading to a non-vanishing radial motion of the plasma column, and where a velocity-dependent viscous force is included, needs further investigation to be reported elsewhere [5].

This section is ended by considering the fluxes of ions and electrons in the case $\boldsymbol{v} \equiv 0$, as given by the intermediate members of (19) and (20) which result in

$$\begin{aligned} \operatorname{div}(n\boldsymbol{v}_i) &= (m_e/e\,m)\,\boldsymbol{u}_B \cdot \nabla p \\ &= -(m_e/m_i)\operatorname{div}(n\boldsymbol{v}_e), \end{aligned} \tag{25}$$

where

$$\boldsymbol{u}_B = (2\boldsymbol{B}/B)^3) \times \nabla B + (1/B^2)\operatorname{curl}\boldsymbol{B}. \tag{26}$$

The quantity $\boldsymbol{u}_B$ demonstrates the relationship between fluid and orbit theory. It includes the contributions to the guiding centre drift from the inhomogeneity of $|\boldsymbol{B}|$ and from the curvature of the magnetic field lines. The guiding centre drifts do not only produce a translation of the charged particles but can also give rise to compression or expansion of the ion and electron fluids. All these effects are taken care of in the macroscopic fluid theory and need not be discussed further in detail. It should only be observed that the axial losses of particles in the case $\boldsymbol{v} = 0$ are given by the current density $\boldsymbol{j}$ only, as expected from simple physical arguments based on orbit theory and shown by (19), (20) and (13).

5. Heat Balance

5.1. Basic Equations of a Fully Ionized Linear Plasma Column

With the result $\boldsymbol{v} \equiv 0$ of Sect. 4.2, (18) can be used to rewrite the left-hand members of (9) and (10) yielding

$$\begin{aligned} &[m_e\,k\,j/e\,m(T_i + T_e)] \\ &\cdot\left[\left(\frac{5}{2}T_i + \frac{3}{2}T_e\right)\frac{\partial T_i}{\partial z} + T_i\frac{\partial T_e}{\partial z}\right] \\ &= 3e^2 n^2 \eta (k/m_i)(T_e - T_i) - \lambda\,\eta\, j^2 + \Pi_t \end{aligned} \tag{27}$$

$$\begin{aligned} &-[m_i\,k\,j/e\,m(T_i + T_e)] \\ &\cdot\left[T_e\frac{\partial T_i}{\partial z} + \left(\frac{3}{2}T_i + \frac{5}{2}T_e\right)\frac{\partial T_e}{\partial z}\right] \\ &= -3e^2 n^2 \eta (k/m_i)(T_e - T_i) + \eta\, j^2 - \Pi_r, \end{aligned} \tag{28}$$

where $j = |\boldsymbol{j}| = j_z$ and $\lambda \equiv \operatorname{div} \boldsymbol{q}_i/\eta j^2$. The condition $v_z = 0$ makes the ions move much more slowly from the anode side into the plasma column than the electrons are moving in the opposite direction from the cathode side. This accounts for the factors m_e/m and $-m_i/m$ in front of the left-hand members.

In the limiting case $T_i \cong T_e \equiv T$ of very strong thermal coupling between ions and electrons, the sum of (27) and (28) gives the heat balance relation

$$-[5(m_i - m_e)kj/2em]\frac{\partial T}{\partial z} = (1-\lambda)\eta j^2 + \Pi_t - \Pi_r \tag{29}$$

which is also obtained from (15) in combination with (18). A relation of similar form can also be deduced by means of simple arguments based on orbit theory and being independent of the restrictions imposed on MHD theory.

The boundary conditions of (27)—(29) in the axial direction are based on the following arguments:

(i) The anode is assumed to be located at $z = 0$ and the cathode at $z = z_a + L + z_c$. Near the anode and cathode, i.e. in the regions $0 < z < z_a$ and $z_a + L < z < z_a + L + z_c$, there are partially ionized layers of small thickness z_a and z_c as compared to the column length L.

(ii) The electrons are created in the cathode region and leave the cathode layer at a temperature $T_b \cong 5 \times 10^4$ K.

(iii) When moving in the negative z direction, the electrons become subject to ohmic heating. Due to the slow ion motion, and provided that this heating is stronger than the rate of heat loss, we expect the electrons to become hotter when moving away from the cathode in the negative z direction. The ions are almost static and nearly adopt the local electron temperature.

(iv) The ions are created in the anode region and leave the interface $z = z_a$ between the anode layer and the fully ionized plasma at a temperature $T_i(z_a) \cong T_b$. When entering the fully ionized plasma region, they meet the hot counterstreaming electrons and are rapidly heated to a temperature being close to that of the electrons. Consequently, the ion and electron temperatures can differ appreciably only within a narrow anode region of thickness z_a which extends from the plane $z = 0$ in the positive z direction. The highest ion temperature is expected to arise near the "interface" $z = z_a$ between this region and the main part of the plasma column within which usually $T_i \cong T_e$. Further modifications of the temperature distributions near the electrode surfaces arise from neutral gas interaction, as discussed later in Section 5.4.

5.2. A Simplified Model for the Axial Heat Balance

With $\boldsymbol{v} \equiv 0$ and $\boldsymbol{j}$ in the axial direction, $\operatorname{div} \boldsymbol{q}_i = \lambda \eta j^2$ represents the only transverse heat loss by conduction and convection appearing in (27)—(29). This loss is covered by the fraction λ of the Ohmic heating power. The remaining fraction $1 - \lambda$ of ηj^2 and the thermonuclear power Π_t then balance the radiation losses Π_r and the axial heat losses due to electrons and ions which drift to the electrodes. Since $v_z = 0$, the latter losses are determined by the current density $\boldsymbol{j}$.

To obtain first-order numerical indications on the axial heat balance and the corresponding axial temperature distributions, a simple model is now adopted in which λ is treated as a constant. Here the hottest inner regions of the plasma near the axis are of particular interest, i.e. where MHD theory becomes inapplicable according to Section 2. However, on account of the large Larmor radii in these regions, we expect the radial temperature and density profiles to become flattened near the axis. Application of (27)—(29) at the outer edge of these "non-MHD" regions is therefore justified for temperatures and densities not being too far from those prevailing at the axis. In this simplified model we finally introduce $\bar{j} = J/\pi \bar{a}^2$ and the average beta value

$$\beta = 8k n_0 (T_{i0} + T_{e0})/\mu_0 (\bar{a}\bar{j})^2 \tag{30}$$

which is close to unity in the present high-beta scheme.

5.3. Limiting Case of Equal Ion and Electron Temperatures

In a high-beta plasma where ohmic heating is a major heat source, the deviation

$$\delta = |T_e - T_i|/(T_e + T_i)$$

from temperature equipartition can be estimated from (9) and (10). At equilibrium the average value of the heat transfer rate

$$\Pi_{ie} = 3e^2 n^2 \eta (k/m_i) |T_e - T_i|$$

between ions and electrons cannot exceed that of the heat production rate $\Pi_\eta = \eta j^2$. In terms of an order-of-magnitude estimate, and in combination with (13), this implies that $\Pi_{ie}/\Pi_\eta \cong \delta(\bar{a}/\bar{a}_i)^2 < 1$. For an efficiently contained plasma the average ion Larmor radius $\bar{a}_i$ should further satisfy the condition $(\bar{a}_i/\bar{a})^2 \ll 1$ within the main parts of the plasma body. Consequently, we expect $\delta \ll 1$, at least within these parts, i.e. where MHD theory can be applied according to Section 2. The limiting case $T_i \cong T_e$ therefore appears to be a good approximation. A detailed numerical example on the axial ion and electron temperature distributions is later presented in Section 6.1.

In an ohmically heated plasma with negligible thermonuclear power production and small radiation losses, integration of (29) in the case $T_i \cong T_e \cong T$ now yields the distribution (compare also Haines [4])

$$T(z) = [T_b^{5/2} + (1-\lambda)\, T_\eta^{5/2}(1 - z/L)]^{2/5} \quad (31)$$

near the axis where

$$T_\eta = [e\, k_\eta\, m L j/(m_i - m_e)\, k]^{2/5}. \quad (32)$$

With $T_b \ll T_\eta$ a maximum temperature $T(z = z_a) \cong T_\eta(1-\lambda)^{2/5}$ is then obtained.

For a plasma heated by thermonuclear reactions, (29) is integrated to

$$L \cdot j \cong \frac{5\, k (m_i - m_e)}{2\, e\, k_\eta\, m} \int_{T_b}^{T(z_a)} \frac{T^{3/2}\, dT}{1 - \lambda + c_t(\varrho_t/\sqrt{T}) - C_r}. \quad (33)$$

Here the coefficients are given by

$$c_t = \mu_0^2 \beta^2 J^2 f_\alpha\, k_t/256\, \pi^2 k^2 k_\eta = f_\alpha\, k_t\, C_r/k_{rb} \quad (34)$$

with β being treated as a constant in a first approximation. In eq. (33) cyclotron radiation has been neglected for three reasons. First, it becomes comparable to the bremsstrahlung loss only at the highest temperature within the ranges specified in Section 3.1.(vi). Second, the magnetic field becomes relatively weak within the hot parts of the plasma near the axis. Third, cyclotron radiation can be reflected by surrounding metal walls and reabsorbed in the plasma. Relation (33) between $L \cdot j$ and T expresses the balance between the net heat production and the end losses from the plasma column. The Pease limit [13] results from $C_r = 1$, $\beta = 1$.

5.4. The Partially Ionized Electrode Layers

The contributions from Π_t and Π_r are neglected in the electrode layers. In analogy with (29) we use the results of Sect. 3.4 to estimate the influence of neutral gas and write

$$\partial T/\partial z = [2\, e\, m/5(m_i - m_e)\, k j] \cdot [n\, n_{na}\, Q_n \exp(-n\, \sigma_{cf}\, z) - (1-\lambda)\, \eta j^2] \quad (35)$$

for the anode region. Within the present parameter ranges it can be seen that Π_n becomes larger than ηj^2 only at small distances from the plane $z = 0$. This implies that T increases here when moving away from the anode. The conditions are analogous in the cathode layer.

The presence of neutral gas in the electrode layers therefore keeps the plasma temperature low in the regions close to the electrode surfaces. In this connection it should be investigated whether the plasma-electrode interaction can be reduced by terminating the straight pinch configuration by "end vessels" containing the electrodes, and where at least the partially ionized plasma can have a larger geometrical cross section than that of the fully ionized column.

6. Numerical Examples

6.1. Unequal Ion and Electron Temperatures

There are, in principle, two mechanisms which give rise to a difference between the ion and electron temperatures in the present system. The first is due to an unbalance between the local heat sources and sinks. The second mechanism originates from the convective axial motion of the charged particles in presence of axial temperature gradients. This produces large temperature gradients close to the anode, as described earlier in Section 5.1.(iv).

The behaviour of an ohmically heated plasma in which Π_t and Π_r are neglected can be demonstrated by numerical integration of (27) and (28), with the approximation of constant β being introduced. An example is chosen with $A = 1$, $j = 2 \times 10^8$ A/m^2, $\bar{a} = 10^{-2}$ m, $\beta = 0.5$, $\lambda = 0.12$, $T_i(z_a) = 5 \times 10^4$ K, $T_e(z_a) = 10^6$ K, $T_e(z_a + L) = 5 \times 10^4$ K, and $z_a \ll L$. The corresponding length L can then be computed from (27) and (28). Here the plasma column is divided into two regions:

(i) Within the region close to the anode, the boundary conditions at $z = z_a$ and the finite value

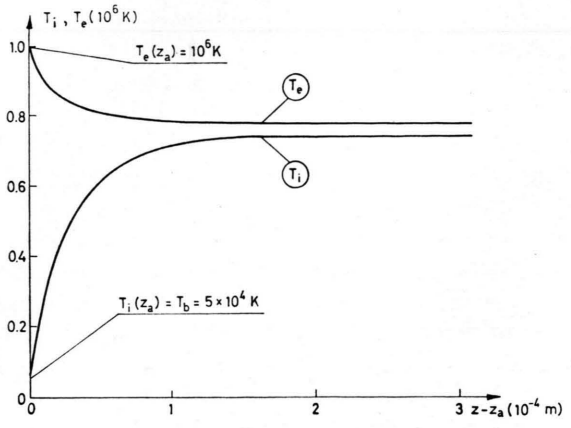

Fig. 2. Formal solution of the axial temperature profiles of ions and electrons near the pinch axis, in a region being close to the anode and with $A = 1$, $j = 2 \times 10^8$ A/m^2, $\bar{a} = 10^{-2}$ m, $\beta = 0.5$, $\lambda = 0.12$.

of the ion current result in a large difference between the ion and electron temperatures, as shown by Figure 2. The large corresponding temperature gradients in this region lead to a rapid decrease of $(T_e - T_i)/(T_e + T_i)$ down to a few percent, already at axial distances exceeding some 10^{-4} m. This behaviour should only be considered as a formal solution of (27) and (28) which becomes modified in several ways near the anode. Thus, the finite Larmor radii tend to broaden this region and reduce its temperature gradients. Further, the presence of neutral gas at the anode reduces both the ion and electron temperatures and affects their gradients as outlined later in Section 6.3.

(ii) At distances from the anode exceeding some 10^{-3} m, the solution of (27) and (28) becomes as demonstrated by Fig. 3 where the axial length $L = 0.129$ m corresponds to the adopted boundary values of T_i and T_e. This solution deviates by less than 4 percent from the result obtained from expressions (31) and (32) which yield

$$T_i \cong T_e \cong 0.74 \times 10^6 \text{ K}$$

close to the anode, i.e. at $z = z_a$.

With the exception of the region close to the anode, the example of Figs. 2 and 3 thus shows that the temperature deviation

$$\delta = (T_e - T_i)/(T_e + T_i)$$

becomes small, as expected from the discussion of Section 5.3.

6.2. *Equal Ion and Electron Temperatures*

In the limit of equal ion and electron temperatures represented by (31)—(34), the following results are obtained:

(i) The case of pure ohmic heating is demonstrated by the characteristic temperature T_η as given by Figure 4. It is expected from the figure and from (31) that comparatively high temperatures can be reached within a considerable fraction of the plasma column length, even in devices of modest scale.

(ii) The case of a subsidiary heating by thermonuclear reactions is demonstrated by Fig. 5 where $J = 2.8 \times 10^6$ A, $\bar{a} = 10^{-2}$ m, $\beta = 0.5$, $\lambda = 0.19$, and a mean value $A = 2.5$ has been introduced for a deuterium-tritium mixture. Due to the discussion of Sect. 5.3, the temperature deviation δ is expected to become small for a contained plasma, at

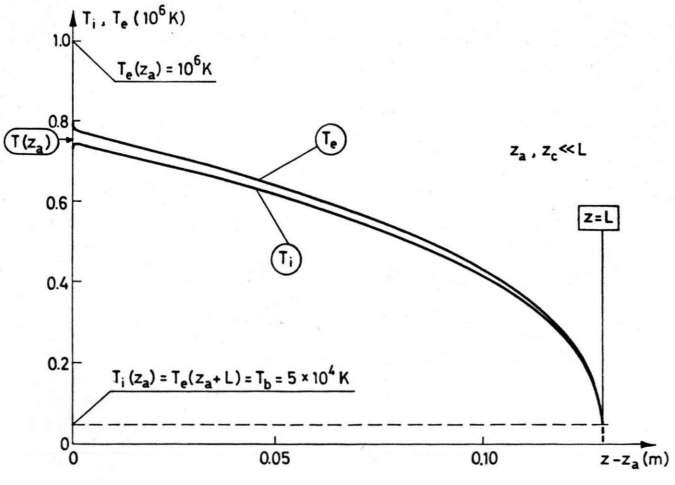

Fig. 3. Same data as in Fig. 2 but showing the axial temperature profiles along the entire plasma column.

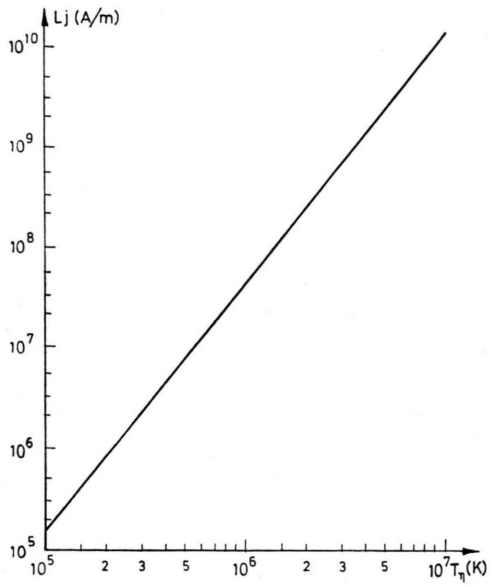

Fig. 4. The characteristic temperature T_η of ohmic heating given by eq. (32) as a function of the product $L \cdot j$ between the column length L and the current density j.

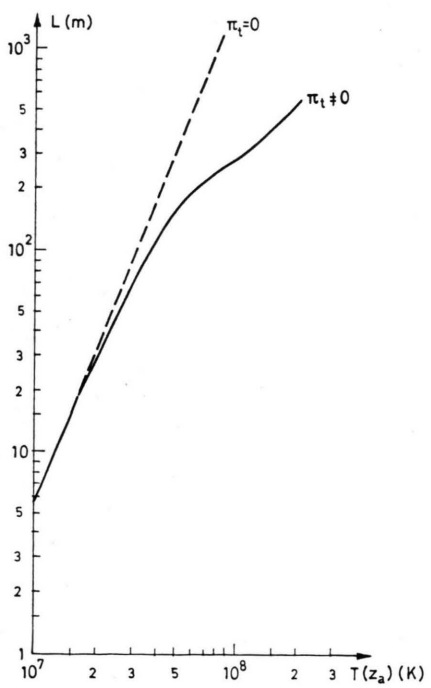

Fig. 5. The maximum temperature $T(z_a)$ as a function of the effective length L of a plasma column with $J = 2.5 \times 10^6$ A, $\beta = 0.5$, $\lambda = 0.19$, $A = 2.5$, and $\bar{a} = 10^{-2}$ m. Full curve represents the balance which would result in presence of alpha particle heating and broken line the case in absence of such heating. The Pease limit is somewhat exceeded here, due to the fact that $\beta < 1$.

least as long as ohmic heating provides a substantial fraction of the total heating power. In Fig. 5 thermonuclear reactions become important at temperatures T above some 2×10^7 K. To reach this temperature, the plasma column should have a length of about 30 m, with a steady-state potential drop of about 3 kV between the electrodes. The alpha particle power would then become about 100 MW/m. These data predict that conditions near ignition could become realizable when the plasma remains stable during the pulse time and the electrode regions do not introduce impurities which lower the plasma temperature substantially. The current density in such an experiment becomes appreciable, i.e. $j \cong 8 \times 10^9$ A/m^2, and it would have to be imposed at ion densities of the order of $n = 10^{24}$ m^{-3}. Finally, with the present data, the Larmor radius of 3.5 MeV alpha particles at the plasma boundary becomes somewhat smaller than $\bar{a}$. Thus, a substantial fraction of these particles should be contained and thermalized within the plasma. The axial alpha particle drift needs further analysis.

6.3. Temperature Gradient in the Electrode Layers

The heat balance conditions in the partially ionized anode layer are roughly given by (35). From an earlier analysis of the plasma-neutral gas balance in a wall layer [14], the ratio between the ion and neutral particle densities near a wall surface is found to be of the order of $(T_n/T_i)^{1/2}$, at a local neutral gas temperature T_n. Further, the deduced layer thickness becomes quite small, i.e. of the order of $d_w = (k T_i/2\pi m_i)^{1/2}/n\xi$.

We shall not enter into a detailed discussion of the complicated balance in the anode layer, but only illustrate (34) by an example with $A = 1$,

$$j = 2 \times 10^8 \text{ A/m}^2, \quad T \cong 5 \times 10^4 \text{ K},$$
$$\xi \cong \xi_{max} \cong 10^{-14} \text{ m}^3/\text{s},$$

and $n \cong n_{na} \cong 10^{23}$ m^{-3}. Then

$$\partial T/\partial z = 10^{10}[\exp(-2 \times 10^4 z) - 8 \times 10^{-3}] \text{ K/m}.$$

Lower values of T are likely to occur close to the anode surface, leading to a smaller effective cross-section σ_{cf} and a larger penetration length of the neutral gas, with a corresponding effect on $\partial T/\partial z$.

In any case, these data indicate that there can exist a narrow partially ionized region near the anode surface within which a steep increase in the ion and electron temperatures takes place in the positive z direction.

7. Conclusions

Provided that a stable state of a clean plasma can be reached during a sufficiently long time, the following conclusions can be drawn about the potentialities of the present linear confinement scheme:

(i) In a purely transverse field there is a reduced transport of particles and heat to the ends of linear configurations, thus allowing for axial temperature gradients. These configurations provide an alternative to open bottles such as mirror devices.

(ii) The present scheme has larger losses than several types of closed toroidal schemes, but it should still become important to fusion research. As compared to toroidal schemes it has the advantages of easily realizable steady operation at high power inputs and beta values, of a geometry without toroidal curvature effects, and of technical simplicity.

(iii) There exist equilibrium states with vanishing axial and radial mass motion. In absence of axial motion the transport of impurities from the end electrodes into the plasma becomes delayed.

(iv) High plasma temperatures are available by means of ohmic heating at moderately large column lengths. Conditions near thermonuclear ignition even appear to become possible at realistic parameter values. Whether reactor schemes can be based on the linear configurations is an open question, partly due to the problems of stability, the large wall load in the present parameter ranges, of plasma-wall interaction at the end electrodes, alpha particle containment and auxiliary heating.

(v) The problems of anomalous transport in these high-beta systems require further investigation, as well as the influence of impurity radiation. A more detailed analysis on plasma-neutral gas interaction is also needed.

8. Acknowledgements

The author is indebted to Drs. T. Hellsten, M. Tendler and E. Tennfors for valuable discussions. Also the help with the numerical calculations of Sect. 6.1 by Dr. B. Bonnevier and Mr. S. Holmberg is gratefully acknowledged.

This work has been financially supported by the European Communities under an association contract between Euratom and Sweden.

[1] A. Schlüter, International School of Fusion Reactor Technology, 5th Course: Unconventional Approaches to Fusion, Erice, 16—25 March 1981.
[2] B. Lehnert, International School of Fusion Reactor Technology, 5th Course: Unconventional Approaches to Fusion, Erice, 16—25 March 1981.
[3] J. R. Drake, T. Hellsten, R. Landberg, B. Lehnert, and B. Wilner, Eighth International Conference on Plasma Physics and Controlled Nuclear Fusion Research, Brussels, 1—10 July 1980, paper IAEA-CN-38/AA-3.
[4] M. G. Haines, Proc. Phys. Soc. **77**, 643 (1960).
[5] M. Tendler, Royal Institute of Technology, Stockholm, TRITA-PFU-81-05 (1981).
[6] A. Schlüter, Z. Naturforsch. **5a**, 72 (1950) and **6a**, 73 (1951).
[7] S. I. Braginskii, Reviews of Plasma Physics, Vol. 1, Consultants Bureau Enterprises, New York 1965.
[8] L. Spitzer, Physics of Fully Ionized Gases, Interscience Publ., New York 1962.
[9] B. Lehnert, Royal Institute of Technology, Stockholm, TRITA-PFU-78-06 1978.
[10] F. L. Ribe, Rev. Mod. Phys. **47**, 7 (1975).
[11] D. J. Rose and M. Clark, Plasmas and Controlled Fusion, Chapt. 11, MIT Press and Wiley 1961.
[12] B. Lehnert, Physica Scripta **12**, 327 (1975).
[13] R. S. Pease, Proc. Phys. Soc. B, **70**, 11 (1957).
[14] B. Lehnert, Ark. Fysik **28**, 499 (1968).